Available online at www.sciencedirect.com
ScienceDirect
International Journal of Mass Spectrometry 265 (2007) 326–336
International Journal of Mass Spectrometry
www.elsevier.com/locate/ijms

An ab initio direct dynamics simulation of protonated glycine surface-induced dissociation

Kyoyeon Park [a], Kihyung Song [a,*], William L. Hase [b,*]

[a] Department of Chemistry, Korea National University of Education, Chongwon, Chungbuk 363-791, Republic of Korea
[b] Department of Chemistry and Biochemistry, Texas Tech University, Lubbock, TX 79409-1061, United States

Received 2 November 2006; received in revised form 9 March 2007; accepted 11 March 2007
Available online 14 March 2007

Abstract

A QM + MM direct dynamics simulation, using MP2/6-31G* theory as a model for the intramolecular potential of protonated glycine (gly-H^+), is used to study gly-H^+ + diamond {1 1 1} SID. The simulations are performed for collisions normal ($\theta_i = 0°$) and oblique ($\theta_i = 45°$) to the surface and at a collision energy of 70 eV (1614 kcal/mol). The gly-H^+ energy-transfer dynamics, observed in this study, are in accord with previous studies in which AMBER and AM1 were used for the ion's intramolecular potential [S.O. Meroueh, Y. Wang, W.L. Hase, J. Phys. Chem. A 106 (2002) 9983]. A particularly important finding is that a significant fraction of the gly-H^+ ions fragment by a shattering mechanism as they collide with the surface. This result supports earlier studies in which shattering fragmentation was also observed for both gly-H^+ and gly_2-H^+, in QM + MM direct dynamics simulations in which the AM1 semiempirical QM model was used for the ion's intramolecular potential, instead of the MP2/6-31G* model. Using MP2/6-31G* the predominant shattering fragmentation channels, in decreasing order of importance, are $NH_3 + CH_2COOH^+$, $NH_3 + CO + CH_2OH^+$, $H_2 + NH_2CHCOOH^+$, and $NH_2CH_2^+ + C(OH)_2$ for $\theta_i = 0°$, and $NH_3 + CH_2COOH^+$, $NH_2CH_2^+ + C(OH)_2$, $NH_2CH_2^+ + HCOOH$, and $NH + C(OH)_2CH_3^+$ for $\theta_i = 45°$. SID at $\theta_i = 45°$ was studied previously with AM1 and the percentage of gly-H^+ trajectories which shatter with MP2/6-31G* is the same as found for AM1.

Keywords: Surface-induced dissociation (SID); Chemical dynamics simulations; Ab initio direct dynamics; Protonated glycine

1. Introduction

Collisions of gaseous particles with surfaces represent a rapidly growing area of chemistry and physics with a wide range of applications in various branches of science and technology. When a polyatomic ion collides with a surface, it can dissociatively or non-dissociatively scatter, stick to the surface, i.e., became trapped on the surface, so-called "soft-landing", or implant into the bulk. Surface-induced dissociation (SID), first introduced by Cooks and co-workers in the 1980s [1], is a mass spectrometry technique for fragmenting and analyzing ions by colliding them with surfaces [1–5]. The specific fragments produced provide detailed information concerning the ion's structure and associated energetics for its fragmentation pathways.

SID has proven to be a successful means to activate and fragment protonated peptides [6–17]. It provides sequence information for peptides, including large multiply charged peptides [18]. High internal energy deposition provided by ion-surface collisions yields extensive fragmentation of protonated peptides, allowing relatively rapid and uncomplicated analyses of their sequences. SID combined with electrospray ionization (ESI) provides a distinct experimental technique to determine the energetics and mechanisms of peptide fragmentation [19]. The relative position of ESI/SID fragmentation efficiency curves (plots of percentage fragmentation versus laboratory collision energy) for peptides can be utilized to estimate relative energetics of peptide fragmentation and predict proton localization sites.

The efficiency of transfer of the collision translational energy to the projectile ion's internal energy, during its collision with the surface, has been investigated by classical trajectory simulations [20–29]. These SID simulations have investigated collisions of $Si(CH_3)_3^+$, $Cr^+(CO)_6$ and protonated polyglycine and polyalanine ions [i.e., gly-$_n$$H^+$ and ala_n-H^+, n = 1–5] with diamond

* Corresponding authors. Tel.: +1 806 742 3152; fax: +1 806 742 1289.
E-mail addresses: ksong@knue.ac.kr (K. Song), bill.hase@ttu.edu (W.L. Hase).

1387-3806/$ – see front matter © 2007 Elsevier B.V. All rights reserved.
doi:10.1016/j.ijms.2007.03.009

{1 1 1} and hydrogenated alkanethiolate self-assembled monolayer (H-SAM) surfaces. These simulations have given an atomic-level understanding of the dynamics of the collisional energy-transfer process. Semiquantitative agreement is found between experimental energy-transfer efficiencies [5,30–32] and those determined from the simulations [33].

The simulations show that ions, including protonated peptides, may fragment by two mechanisms. The first dissociation mechanism corresponds to the traditional RRKM mechanism [34]. The ions initially undergo impulsive excitation upon collision with the surface, are inelastically reflected off the surface, and then undergo unimolecular dissociation. The collisionally excited ion first rebounds off the surface and then dissociates after intramolecular vibrational energy redistribution (IVR). At low collision energies, the experimental kinetic to internal energy-transfer efficiencies are fit to an implusive excitation model which quantitatively duplicates the dependence on both the initial kinetic energy and effective mass of the surface [3]. The second dissociative mechanism corresponds to so-called "shattering", in which the ion dissociates as it collides with surface. Experimental evidence in support of both these mechanisms has been observed for different ions [35,36], including peptide ions [37–39].

The previous calculations, which identified a shattering mechanism for gly-H^+ and gly_2-H^+ fragmentation [24,27], were QM + MM direct dynamics simulations [40,41]. The AM1 semiempirical quantum mechanical (QM) theory was used to represent the potential energy function for the peptide ion V_{ion}. The complete potential energy function for the simulations is written as

$$V = V_{ion} + V_{surf} + V_{ion-surf} \quad (1)$$

where V_{surf} is the potential for the model of diamond {1 1 1} used in the simulations and $V_{ion\text{-}surf}$ is the peptide ion surface intermolecular potential. Both V_{surf} and $V_{ion\text{-}surf}$ are analytic molecular mechanical (MM) type potentials.

Though AM1 theory gives an overall good representation of potential energy barriers for gly-H^+ dissociation [24], it is not as accurate as higher levels of theory such as the B3LYP and MP2 methods (see Table 1 in Ref. [24]). A similar difference between AM1 and B3LYP and MP2 is expected for gly_2-H^+ and larger peptides. Given the importance of unequivocally characterizing fragmentation mechanisms for peptide ion SID, it is important to perform the simulations at higher levels of theory than AM1. This is computationally feasible for small peptides and, in the work presented here, a QM + MM direct dynamics simulation of gly-H^+ diamond {1 1 1} SID is reported. The simulation is identical to the previous study [24], except MP2/6-31G* is used for the V_{ion} potential instead of AM1. In addition, more atomic-level details are given for the energy transfer and fragmentation dynamics.

2. Potential energy function

The model used in this study for the gly-H^+ + diamond {1 1 1} system is the same as that used previously [24] and it consists of a 1988 atom diamond surface. The potential energy function is given in Eq. (1). As described above, the MP2/6-31G* electronic structure theory model was used for the gly-H^+ intramolecular potential. The remaining potentials are analytic functions, described in detail previously [23,42]. The potential energy function for the diamond {1 1 1} model consists of harmonic stretches and bends, with force constants chosen to fit the diamond phonon spectrum [42]. The ion-surface intermolecular potential, $V_{ion\text{-}surf}$, is modeled by a sum of two-body potentials between the atoms of the peptide and the atoms of the surface. The two-body potential is given by

$$V_{XY} = A_{XY} \exp(-B_{XY} r_{ij}) + \frac{C_{XY}}{r_{ij}^6} \quad (2)$$

where X corresponds to the C and H atoms of diamond and Y corresponds to the H, C, O, and N atoms of the peptide. To determine the parameters for the two-body potentials, ab initio potential energy curves were calculated [23] using CH_4 for the C and H atoms of diamond and CH_4, NH_3, NH_4^+, H_2CO, and H_2O as models for the different types of atoms and functional groups comprising peptides. In fitting the ab initio potentials with a sum of two-body potentials, as given by Eq. (2), the focus was on accurately fitting the short-range, repulsive region of the two-body potential [23]. The long-range region is not sufficiently attractive and obtaining two-body potentials which accurately fit both the short-range and long-range regions is an important current research project [43].

3. Computational procedure

The direct dynamics classical trajectory simulations were carried out with general chemical dynamics computer program VENUS [44] interfaced with the electronic structure theory computer program Gaussian [45]. Initial conditions for the trajectories were chosen to represent experiments, as described in the previous study [24]. Gly-H^+ was randomly rotated about its center-of-mass to sample all collision orientations and directed, with a random azimuthal angle, towards a randomly chosen impact site on the surface. Initial conditions, for a 300 K Boltzmann distribution, were chosen for the vibrational modes of gly-H^+ using the quasiclassical normal mode method [46].

Initial conditions for the diamond surface were chosen by assigning velocities sampled from a 300 K Maxwell–Boltzmann distribution for the surface of atoms. The surfaces were then equilibrated for 2 ps of molecular dynamics by scaling the velocities [47] so the temperature corresponds to that for a 300 K classical Boltzmann distribution. The structure obtained from this equilibration process is then used as the initial structure for 0.1 ps equilibration run at the beginning of each trajectory. A total of 544 and 116 trajectories were calculated, using a 6th order symplectic integrator [48], for a collision energy E_i of 70 eV and an incident angle θ_i of 0° and 45°, respectively, with respect to the surface normal. The trajectories were initiated with a 16 Å separation between the gly-H^+ center-of-mass and the top of the surface and terminated when this separation exceeded 20 Å. To calculate a trajectory that terminated in this manner

required ~20–30 h of CPU time on a single processor 3.0 GHz Pentium IV computer.

This trajectory ensemble was initially propagated with an integration step-size of 2 fs, and, for $\theta_i = 0^\circ$, 114 of the trajectories had either an error in the numerical integration (i.e., discontinuity in the MP2/6-31G* energy) or a SCF convergence failure. These 114 trajectories were rerun with integration step-sizes of 1 fs and smaller, and 34 ended normally with a separation between both the nitrogen and hydroxyl oxygen of gly-H^+ and the top center atom of the surface greater than 20 Å. Among these, 33 trajectories could be analyzed for both the final energy partitioning and the gly-H^+ fragmentation pattern. One trajectory had one carbon atom remaining near the surface, and thus excluded from the final energy analysis. The remaining 80 trajectories terminated as the result of a numerical integration error or SCF convergence failure. Of these, 63 terminated after scattering off the surface and their fragmentation mechanisms could be identified. The remaining 17 terminated as gly-H^+ hit the surface and their fragmentation products could not be identified. Most of the convergence failure trajectories fragmented via channels forming OH^+, H^+, or the H-atom.

Of the above 63 trajectories, 28 terminated sufficiently above the surface that the gly-H^+/surface interaction energy was small and, thus, very accurate final energies could be calculated. For the remaining 35 trajectories, their fragmentation mechanisms could be identified as described above, but they terminated too near the surface to determine final energies.

To summarize, a total of 544 trajectories were calculated. The fragmentation mechanism was identified for all but 17 of the trajectories and the final energy analysis was possible for all but 53. The final energies are identified by

$$E_i = E_f + \Delta E_{surf} + \Delta E_{int} \quad (3)$$

where E_i is the initial collision energy, E_f the translational energy of the center of mass of the scattered ion (or its fragments), ΔE_{surf} the energy transfer to the surface, and ΔE_{int} is the energy transfer to the gly-H^+ ion's internal vibrational/rotational motions. It should be noted that the number of $\theta_i = 0^\circ$ trajectories with a numerical problem decreased from 114 to 80 when the integration time step was decreased from 2 to 1 fs. With a smaller time step or different integrator the number of trajectories with a numerical problem may be further reduced.

In contrast, of the 116 trajectories with an incident angle of 45°, only 4 terminated by SCF convergence failure. These 4 trajectories were rerun with a 1 fs integration step-size. These trajectories also terminated with a SCF convergence failure, but at sufficient distance above the surface that the final energies as well as fragmentation mechanism could be determined.

The total integration time of the atomic motion for each trajectory varied from 340 to 570 fs. With a 70 eV collision energy and $\theta_i = 0^\circ$, it took gly-H^+ 130 fs to strike the surface. Thus, the time period for which the internal dynamics of excited gly-H^+ was followed is 210–440 fs. For $\theta_i = 45^\circ$ the gly-H^+ internal dynamics was followed for 190–300 fs.

4. Trajectory results

The trajectories were analyzed to determine their fragmentation mechanisms and distributions for the energy transfers to E_f, ΔE_{surf}, ΔE_{int}. Additional analyses were performed to determine the dependence of the energy-transfer distributions and fragmentation mechanisms on the orientation of gly-H^+ as it strikes the diamond surface. The simulations were performed for θ_i of 0° and 45°.

4.1. Energy-transfer efficiencies

The distributions for the collision energy remaining in peptide ion translation, $P(E_f)$, transferred to the surface, $P(\Delta E_{surf})$, and transferred to the ion, $P(\Delta E_{int})$, are plotted in Fig. 1 for θ_i of 0° and 45°. The average percentage energy transfers, determined for these distributions are listed in Table 1, where they are compared with previous results. An important finding, for $\theta_i = 45^\circ$, is that representing V_{ion} by MP2/6-31G* theory gives the same average energy-transfer efficiencies as found previously [24] when representing V_{ion} by AM1 and AMBER. The AM1 and AMBER energy-transfer distributions are the same, within statistical uncertainties [24], and the current MP2/6-31G* distributions given in Fig. 1 are also the same as those for AM1 and AMBER within statistical uncertainties. (The distributions in Fig. 1 may be compared with those in Fig. 7 of Ref. [24].) Thus, AM1, AMBER, and MP2/6-31G* give the same energy-transfer probabilities for gly-H^+ collisions with diamond

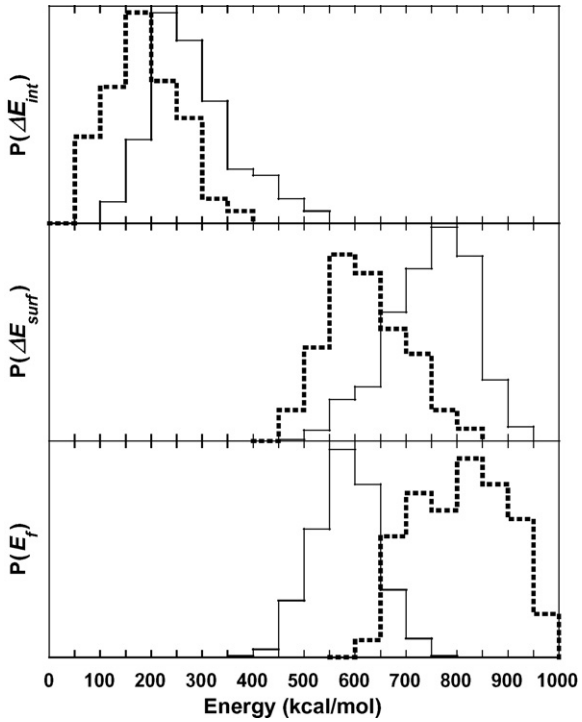

Fig. 1. Distributions of ΔE_{surf}, ΔE_{int}, and E_f for gly-H^+ collisions with diamond {1 1 1} for $E_i = 70$ eV. MP2/6-31G* theory is used for the gly-H^+ intramolecular potential. Solid line, $\theta_i = 0^\circ$, and dashed line, $\theta_i = 45^\circ$. Representative error bars are illustrated in Fig. 3. The total energy to be distributed is $E_i = 70$ eV = 1614 kcal/mol.

Table 1
Energy-transfer efficiencies

Ion, V_{ion}	E_i, θ_i	Average percentage energy transfer			
		ΔE_{int}	ΔE_{surf}	E_f	Ref.
gly-H$^+$, MP2[a]	70, 0°	17.4	46.5	36.1	[b]
gly-H$^+$, MP2[a]	70, 45°	11.4	38.4	50.2	[b]
gly-H$^+$, AM1	70, 45°	12	38	50	[24]
gly-H$^+$, AMBER	70, 45°	11	37	52	[24]
gly$_2$-H$^+$, AM1	70, 0°	20	40	40	[27]
gly$_2$-H$^+$, AMBER	70, 0°	21.7	40.9	37.4	[28]
gly$_2$-H$^+$, AM1	70, 45°	12	27	61	[27]
gly$_2$-H$^+$, AMBER	70, 45°	15.1	24.9	60.0	[28]

E_i is in eV; 70 eV equals 1614 kcal/mol.
[a] QM + MM calculations with the 6-31G* basis set.
[b] This work.

{1 1 1}. That these three models for the gly-H$^+$ potential give the same energy-transfer efficiencies suggests the energy-transfer results from the impulsiveness of the collision [35] and the ion-surface intermolecular potential.

The energy-transfer probabilities for both gly-H$^+$ and gly$_2$-H$^+$ show that changing the incident angle from 0 to 45° decreases energy transfer to the surface and ion, with more of the collision energy remaining in translation. However, with this change in θ_i for gly$_2$-H$^+$, the decrease in energy transfer to the surface and increase in the energy remaining in translation are much larger than found for gly-H$^+$. For the same collision conditions, the percent energy transfer to ΔE_{int} is not significantly different for gly-H$^+$ and gly$_2$-H$^+$. Though the gly$_2$-H$^+$ ion receives more energy transfer, it is only 3–4% larger; e.g., 11% for gly-H$^+$ and 15% for gly$_2$-H$^+$.

4.2. Initial gly-H$^+$ orientation and energy transfer

In the previous simulation study of gly$_2$-H$^+$ + diamond {1 1 1} collisions [28], energy transfer was studied as a function of the orientation of the peptide's backbone as it struck the surface. Since the peptide ion had no rotational energy in the initial conditions, its initial orientation defined its orientation as it collided with the surface. This initial orientation was determined by defining a vector from the nitrogen atom of the protonated amino group to the hydroxyl oxygen atom of the carboxylic group. The angle between this vector and the vector normal to the diamond surface determined the orientation angle Ψ_i of the peptide ion. For Ψ_i of 0° and 180° the backbone of the peptide collides with a vertical orientation, while for $\Psi_i = 90°$ it collides with a horizontal orientation. For the gly$_2$-H$^+$ + diamond {1 1 1} collisions, energy transfer was more efficient for vertical orientations than for horizontal, with energy transfer somewhat more efficient if the C-terminus of the peptide strikes the surface instead of the N-terminus.

The same analysis of energy transfer versus orientation angle was made for this simulation of gly-H$^+$ + diamond {1 1 1} collisions. Since gly-H$^+$ has no initial rotational energy, its initial orientation defines its orientation as it collides with the surface. The orientation angle Ψ_i is defined as described above; i.e., the angle between a vector from the nitrogen atom to hydroxyl oxygen atom of gly-H$^+$ and a vector normal to the surface. In Fig. 2 the internal energy changes for the peptide ion and surface, and the final translational energy, are plotted versus the orientation angle for the gly-H$^+$ + diamond {1 1 1} collisions. The smaller number of points for Ψ_i near 0° and 180° is a reflection of the sin Ψ_i weighting in choosing the initial conditions. As done in a previous study [28], second-order polynomial fits, given by

$$\Delta E_{int} = a(\Psi_i - \Psi_o)^2 + b \quad (4)$$

for ΔE_{int}, were used to establish trend lines for the data. (The fitting parameters are available from the authors on request.) Though there is considerable scatter in the data, the fits indicate orientation has an effect on the gly-H$^+$ energy transfer, but it is not as pronounced as for gly$_2$-H$^+$. As shown in Fig. 4 of Ref. [28], for gly$_2$-H$^+$ + diamond {1 1 1} energy transfer depends strongly on Ψ_i, with the energy transfers to ΔE_{surf} and E_f a maximum at $\Psi_i \approx 90°$ and the energy transfer to ΔE_{int} a minimum at this Ψ_i. One point of agreement between the effects of orientation on the gly-H$^+$ and gly$_2$-H$^+$ collision dynamics is that for both ions energy transfer to ΔE_{int} is most efficient for $\Psi_i = 180°$, with the carboxylic terminus first striking the surface. The much smaller orientation dependence of energy transfer for the gly-H$^+$ collisions, as compared to those for gly$_2$-H$^+$, may be because gly-H$^+$ is a smaller molecule and has a less pronounced backbone. That AM1 and MP2 give the same energy-transfer efficiencies, and very similar fragmentation dynamics (see below), for gly-H$^+$ indicates that the different effect of orientation for gly-H$^+$ versus gly$_2$-H$^+$ energy transfer is not a reflection of using MP2 for gly-H$^+$ and AM1 for gly$_2$-H$^+$.

4.3. Fragmenting and shattering trajectories

For the two simulations reported here, the fractions of trajectories which fragment and shatter are listed in Table 2, where they are compared with the previous simulations for gly-H$^+$ and gly$_2$-H$^+$ with AM1 for V_{ion}. Shattering is identified as an event for which at least one fragmentation occurs as the ion collides with the surface. All the fragmentation may occur during this impact or there may be further fragmentation after the shattering fragments bounce off the surface. The fraction of the trajectories which shatter does not depend on the trajectory integration time.

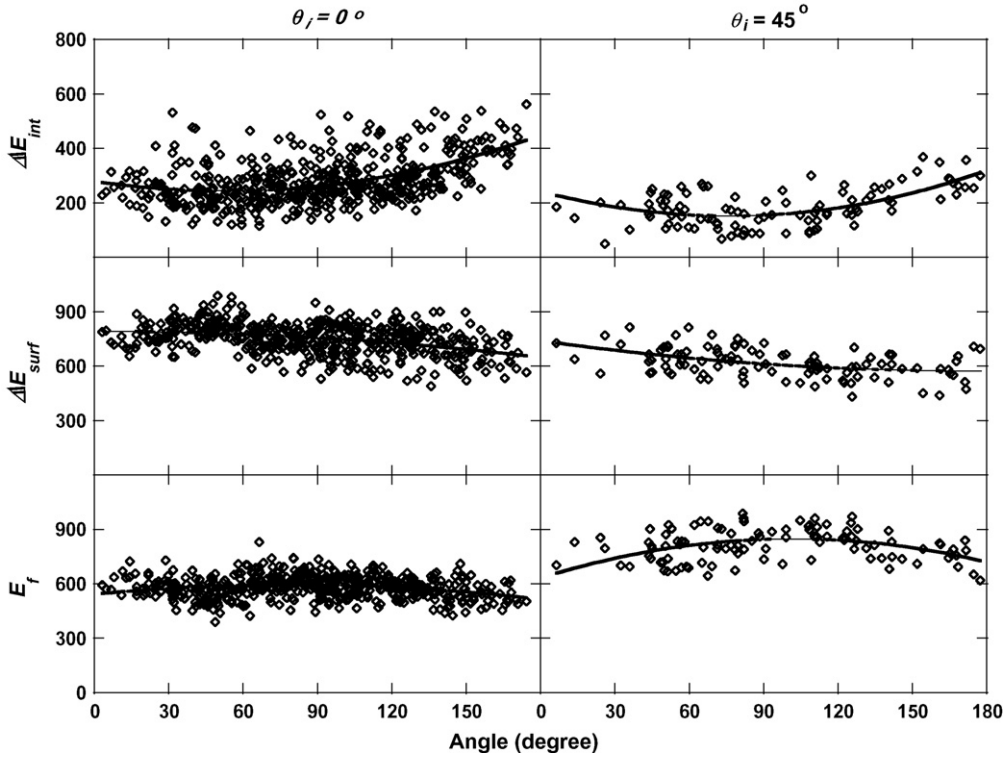

Fig. 2. Scatter plots of the energy transfers in Fig. 1 vs. the gly-H$^+$ orientation angle Ψ_i. The curves are parabolic fits, Eq. (4). Energy is in kcal/mol.

In contrast, the fragmentation fraction depends on the period of time the dynamics of the peptide ion is followed after its collision with the surface. This time is shorter for the current MP2 simulations as compared to the previous AM1 simulations.

A particularly important finding is that the fraction of gly-H$^+$ trajectories that shatter, for $\theta_i = 45^\circ$, is the same for the MP2/6-31G* and AM1 simulations. Comparing the MP2 results for the two θ_i shows that shattering is more likely for $\theta_i = 0^\circ$, which is expected since the perpendicular component of its kinetic energy is larger. There is also less total fragmentation at $\theta_i = 45^\circ$, even though the gly-H$^+$ dynamics is followed for a longer period of time. This results from smaller amounts of ΔE_{int} energy transfer at $\theta_i = 45^\circ$.

A comparison of the MP2 results for gly-H$^+$ and AM1 results for gly$_2$-H$^+$ at $\theta_i = 0^\circ$ shows there is a small decrease in the shattering fraction for the larger ion. The agreement between the MP2 and AM1 shattering fractions for $\theta_i = 45^\circ$ suggests that the same result would have been obtained if MP2 had been used for the gly$_2$-H$^+$ simulation. However, the effect of peptide ion size on the efficiency of shattering is an important issue and in the future it will be important to use MP2 to study SID of larger peptide ions.

The total gly-H$^+$ fragmentation fractions in Table 2 for the MP2 and AM1 calculations are consistent. For MP2, 0.08 of the fragmentation occurs by non-shattering, while this fraction is 0.19 for the AM1 calculation. The larger fragmentation fraction for the AM1 calculation is consistent with the longer time the gly-H$^+$ ion's unimolecular dynamics was followed with AM1, i.e., 1.3 ps versus 0.19–0.30 ps with MP2. It is important to note that if the unimolecular dynamics of the excited gly-H$^+$ ions were followed for a sufficiently long time, all are expected to dissociate. For both the AM1 and MP2 calculations the minimum amount of internal energy transferred to gly-H$^+$ is greater than 50 kcal/mol; i.e., see Fig. 7 of Ref. [24] and the

Table 2
Fractions of fragmenting and shattering trajectories

Molecule (theory)	E_i, θ_i[a]	Time[b]	Number of trajectories	Total fragmenting fraction[c]	Shattering fraction[d]
gly-H$^+$ (MP2/6-31G*)[e]	70, 0°; 70, 45°	0.21–0.44; 0.19–0.30	527; 116	0.68; 0.30	0.57; 0.22
gly-H$^+$ (AM1)[f]	70, 45°	1.3	100	0.42	0.23
gly$_2$-H$^+$ (AM1)[g]	70, 0°	0.85	122	0.66	0.44

[a] Collision energy is in eV; 70 eV equals 1614 kcal/mol.
[b] Maximum period of time (ps) the dynamics of the peptide ion was followed after its collision with the surface.
[c] The total fragmenting fraction includes both shattering and non-shattering events.
[d] Number of trajectories which shatter divided by the total number of trajectories.
[e] Results reported here.
[f] Ref. [24].
[g] Ref. [27].

current Fig. 1. B3LYP/6-31++G** [49], B3LYP/6-31G* [50], MP2/6-31G*[50,51], QCISD(T)/6-31+G** [50], and AM1 [24] calculations predict the lowest barrier for gly-H^+ dissociation is 36–41 kcal/mol to form $NH_2CH_2^+ + CO + H_2O$.

Due to its larger size and more degrees of freedom, amongst which the internal energy may be distributed, less fragmentation might be expected for gly_2-H^+ as compared to gly-H^+ at the same collision energy and incident angle and for the same trajectory integration time [34]. As shown in Table 2, nearly identical fragmentation probabilities are found for gly-H^+ and gly_2-H^+ at the same collision energy and incident angle. However, the unimolecular dynamics of the gly_2-H^+ trajectories were followed for a longer period of time of 0.85 ps as compared to 0.21–0.44 ps for the gly-H^+ trajectories, so that gly_2-H^+ had more time to fragment.

4.4. Initial gly-H^+ orientation and fragmentation dynamics

The probabilities of the different collision events (i.e., fragmentation, non-fragmentation, shattering, and non-shattering fragmentation) are given in Fig. 3 as a function of the peptide ion's orientation angle Ψ_i for the MP2/6-31G* simulations with $E_i = 70$ eV and $\theta_i = 0°$. To remove the $\sin\Psi_i$ weighting factor which is present in selecting the initial conditions [45], the number of trajectories in each bin was multiplied by $1/\sin\Psi_i$, where Ψ_i is the median angle within the bin. Thus, the height of the bin represents the probability the particular event occurred for the specific $\Delta\Psi_i$ bin width. Fragmentation in the top graph is a sum of shattering and non-shattering fragmentation. The ratio of bin heights, for two types of events for the some $\Delta\Psi_i$, equals the ratio of the number of trajectories for the two event types. As discussed above, all of the trajectories are expected to fragment if the trajectories are integrated for a sufficiently long period of time. Thus, the most meaningful analysis in Fig. 3 is for the shattering events.

As shown in Fig. 3, both the shattering probability is largest for vertical or near vertical orientations with Ψ_i approximately equal to 0° or 180°. Concurrent with a greater efficiency for energy transfer to ΔE_{int} for $\Psi_i = 180°$ (i.e., see Fig. 2), shattering is also more probable for $\Psi_i = 180°$ with the carboxylic terminus first striking the surface instead of the protonated amine group. Collisions in which the carboxylic group first impacts the surface clearly promote fragmentation.

4.5. Fragmentation mechanisms

Fig. 4 shows possible backbone cleavage sites for gly-H^+ fragmentation. Site 1 is C–C bond rupture, site 2 C–O bond rupture, and site 3 C–N bond rupture. In addition, C–H bond rupture was observed and identified as site 4. The probabilities for the different backbone cleavage patterns observed in the trajectories are listed in Table 3 for the calculations at θ_i of 0° and 45°. The most probable cleavage pattern is bond rupture at site 1 for both initial angles. Bond cleavages at sites 2 and 3 are much less probable than at site 1 for $\theta_i = 0°$, but for $\theta_i = 45°$ cleavage at sites 2 and 3 have nearly equal probabilities. Multiple backbone cleavages are important for $\theta_i = 0°$, but not for $\theta_i = 45°$.

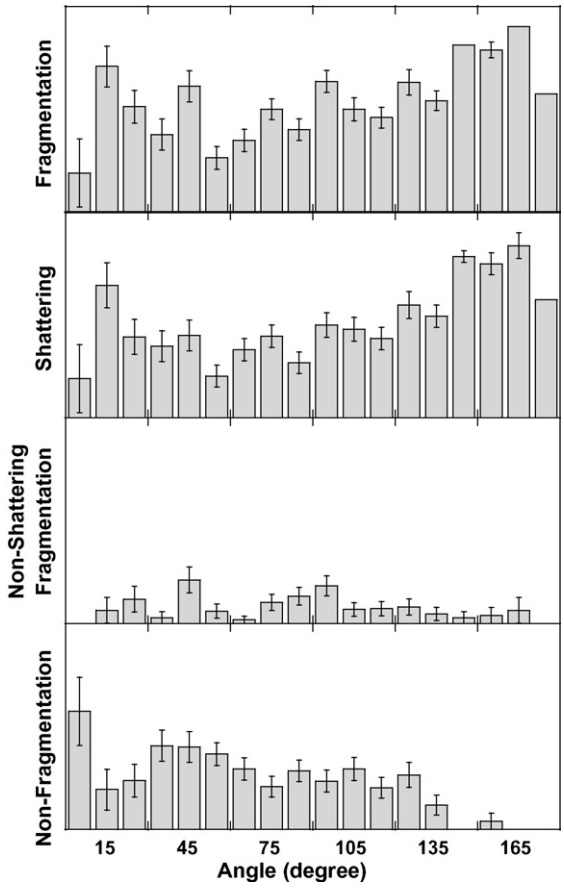

Fig. 3. Probabilities of different gly-H^+ scattering events vs. the gly-H^+ orientation angle Ψ_i for the MP2/6-31G* simulations with $E_i = 70$ eV and $\theta_i = 0°$. The bar height is the number of trajectories in each angle interval, $\Delta\Psi_i = 10°$, divided by $\sin\Psi_i$, where Ψ_i is the median angle within the interval. Dividing by $\sin\Psi_i$ removes the $\sin\Psi_i$ weighting factor present in selecting the initial conditions. The error bars depict the standard deviation in the number of events within each $\Delta\Psi_i$ interval. All the ions are expected to fragment if the trajectories were integrated for a sufficiently long period of time.

The enhanced multiple backbone bond cleavages for $\theta_i = 0°$ is consistent with more energy transferred to the gly-H^+ internal degrees of freedom for perpendicular collisions. H-atom elimination is important for $\theta_i = 0°$, where 130 out of the 138 H-atom eliminating trajectories involved shattering.

As discussed above, for both θ_i's, all of the scattered gly-H^+ ions contain sufficient internal energy to fragment. Thus, if the dynamics of scattered ions were followed for a much longer

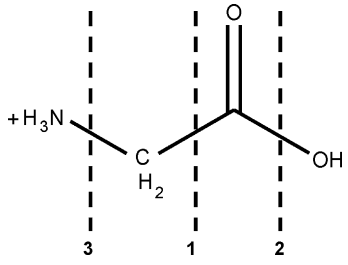

Fig. 4. Possible bond rupture sites for the gly-H^+ backbone. Site 1 is C–C bond rupture, site 2 is C–O bond rupture, and site 3 is C–N bond rupture. C–H bond rupture also occurs, identified as site 4.

Table 3
Number of trajectories which fragment at each dissociation site

Backbone cleavage pattern	Number of trajectories	Number of H elimination[a]	Number of shattering
$\theta_i = 0^\circ$			
1	139 (0.26)[b]	66	105
2	21 (0.04)	3	17
3	39 (0.07)	1	32
1 2	73 (0.14)	25	60
1 3	53 (0.10)	12	49
1 2 3	5 (0.01)	1	5
No backbone cleavage	30 (0.06)	30	30
No reaction	167 (0.32)	–	–
Total	527	138	298
$\theta_i = 45^\circ$			
1	16 (0.14)[b]	2	13
2	1 (0.01)	0	0
3	14 (0.12)	0	10
1 2	2 (0.02)	1	2
1 3	1 (0.01)	0	0
1 2 3	0 (0.00)	0	0
No backbone cleavage	1 (0.01)	0	1
No reaction	81 (0.70)	–	–
Total	116	4	26

[a] H elimination is channel 4 and includes H, H_2, and $H + H_2$ eliminations.
[b] The number in parentheses is the probability of the cleavage pattern.

period of time than the less than 0.5 ps studied here, 100% fragmentation is expected and the backbone cleavage pattern may differ from what is found here. However, the complete shattering fragmentation dynamics is obtained from the current simulation and they may be documented. For $\theta_i = 0^\circ$ the relative ranking by decreasing importance of different backbone shattering patterns is cleavage at site 1; sites 1 and 2; sites 1 and 3; site 3; site 2; and sites 1, 2, and 3. For $\theta_i = 45^\circ$, cleavage of multiple sites by shattering is much less important and only constitutes ~10% of the fragmentation.

Of the 60 $\theta_i = 0^\circ$ shattering trajectories with cleavage at both sites 1 and 2, site 1 shattered as the ion hit the surface for ten of the trajectories and site 2 shattered for seven. The second cleavage occurred after the shattering fragments rebounded off the surface. For 43 of the 60 trajectories, sites 1 and 2 shattered nearly simultaneously. Of the 49 $\theta_i = 0^\circ$ shattering trajectories, which cleaved at sites 1 and 3, 12 shattered simultaneously at these sites yielding H_2. Of these, for 3 these two sites cleaved by shattering, followed by H_2 dissociation, and 9 shattered nearly simultaneously to all the product fragments including H_2. Of the 37 remaining trajectories, 15 shattered at site 3, 1 shattered at site 1, and 21 shattered simultaneously at sites 1 and 2.

Each backbone cleavage resulted in multiple fragmentation channels and the 96 different channels found from the $\theta_i = 0^\circ$ simulations are listed in Table 4 and the 14 different channels found from the $\theta_i = 45^\circ$ simulations are listed in Table 5. Also included are the number of trajectories which fragmented in this manner and the number of the trajectories which are shattering events. The $\theta_i = 45^\circ$ non-perpendicular collisions transfer less collision energy to the internal degrees of freedom of gly-H^+ (see Table 1), which results in substantially fewer fragmentation channels. For $\theta_i = 0^\circ$ the predominant channels in decreasing order of importance are $NH_3 + CH_2COOH^+$, $NH_2CH_2^+ + C(OH)_2$, $NH_3 + CO + CH_2OH^+$, $H_2 + NH_2CHCOOH^+$ and $NH_2CH_2^+ + CO + H_2O$. For $\theta_i = 45^\circ$ the predominant fragmentation channels in decreasing order of importance are $NH_3 + CH_2COOH^+$, $NH_2CH_2^+ + C(OH)_2$, and $NH_2CH_2^+ + HCOOH$. These are well known channels for gly-H^+ fragmentation as found from the previous QM + MM direct dynamics simulation [24], electronic structure calculations [49–52], and experiment [53–55].

The trajectories were followed for a sufficient period of time to identify all shattering events and it is of interest to identify the relative importance of the different shattering pathways. This analysis is summarized in Table 6. For both θ_i's the dominat shattering channel yields $NH_3 + CH_2COOH^+$. However, the relative importance of the lesser channels is different for the two θ_i's. As shown in Table 4 for $\theta_i = 0^\circ$, many of the product channels are only formed by shattering and the strong suspicion is that no additional products would be observed for these channels if the trajectories were followed to complete dissociation. For example $H_2 + NH_2CHCOOH^+$ is one of the dominant channels and appears to be only formed by shattering. The statistics are much poorer for the $\theta_i = 45^\circ$ simulations, but many of the fragmentation channels observed at this angle may also only occur by shattering. Two such channels may be $NH_2CH_2^+ + HCOOH$ and $NH + C(OH)_2CH_3^+$.

Table 6 also provides a comparison of the gly-H^+ shattering dynamics predicted by MP2 and AM1 at $\theta_i = 45^\circ$. For both the $NH_2CH_2^+ + C(OH)_2$ and $NH_2CH_2^+ + HCOOH$ product channels the MP2 and AM1 QM models give similar fragmentation probabilities. However, $NH_3 + CH_2COOH^+$ is the dominant MP2 channel, but much less important for AM1. Similarly, $HNCH_2 + H_2 + COOH^+$ is the dominant AM1 fragmentation

channel, but much less important for MP2. In addition, $NH + C(OH)_2CH_3^+$ is the fourth most important MP2 channel, but not observed in the AM1 simulation. Another important difference between the previous AM1 [27] and current MP2 simulations at $\theta_i = 45°$ is the smaller number of H atom or H_2 shattering channels for the latter. For MP2 3.4% of the trajectories shatter to form H or H_2, while for AM1 the fraction is 13%. For the MP2 simulation all the H and H_2 products were formed by shattering. For AM1 there is one additional non-shattering event forming H_2.

Previous MP2, B3LYP, and QCISD(T) ab initio calculations [49–52], with the 6-31G*, 6-31+G** and 6-31++G** basis sets, have studied the following gly-H^+ fragmentation channels and determined the fragmentation barriers (kcal/mol) given in parenthesis: $NH_2CH_2^+ + CO + H_2O$ (36–41), $NH_2CH_2^+ + C(OH)_2$ (52–63), $NH_3CH_3^+ + CO_2$ (74–78), $NH_2CHCOOH^+ + H_2$ (∼80), and $NH_2CH_2^+ + HCOOH$ (85–93). Each of these

Table 4
Products from gly-H^+ SID for $\theta_i = 0°$

Backbone cleavage pattern	Reaction channel[a]	Number of trajectories	Number of shattering
	no reaction	167	
1	$NH_2CH_2^+ + C(OH)_2$	29	12
1	$NH_2CH_2^+ + HCOOH$	9	6
1	$NH_3CH_2 + CO_2H^+$	9	6
1	$CH_3NH_3^+ + CO_2$	7	5
1	$NH_3CH^+ + HCOOH$	6	5
1	$NH_2CH_3 + CO_2H^+$	5	5
1	$NHCH_2 + CH(OH)_2^+$	3	2
1	$NH_2CHOH^+ + HCHO$	2	0
1	$CH_2(OH)(NH_2) + COH^+$	1	1
1	$CH_2(OH)(NH_3)^+ + CO$	1	0
1	$NH_2CH + CH(OH)_2^+$	1	1
1 4	$H_2 + NH_2CHOH^+ + CO$	9	9
1 4	$H_2 + HCNH^+ + HCOOH$	7	7
1 4	$H_2 + NH_2CH_2^+ + CO_2$	7	4
1 4	$H2 + NHCH_2 + CO_2H^+$	6	6
1 4	$2H_2 + HNC + CO_2H^+$	6	6
1 4	$H_2 + HCN + CH(OH)_2^+$	5	5
1 4	$2H_2 + HCN + CO_2H^+$	4	4
1 4	$H\cdot + NH_2CH_2^+ + CO_2H\cdot$	3	3
1 4	$H^+ + CHOHNH_3 + CO$	2	2
1 4	$H_2 + HNC + CH(OH)_2^+$	2	2
1 4	$H_2 + NH_3CH^+ + CO_2$	2	2
1 4	$H_2 + NH_2CHO + COH^+$	2	2
1 4	$2H + HNCH^+ + C(OH)_2$	1	1
1 4	$2H_2 + CN^+ + C(OH)_2$	1	1
1 4	$2H_2 + HCNH^+ + CO_2$	1	1
1 4	$H + CNH_2 + CH(OH)_2^+$	1	1
1 4	$H + NH_2CH_2^+ + CO_2H$	1	0
1 4	$H^+ + 2H_2 + CN^- + CO_2H^+$	1	1
1 4	$H^+ + NH_2CH + C(OH)_2$	1	1
1 4	$H^+ + NH_3CH_2 + CO_2$	1	1
1 4	$H_2 + H^+ + NH_2COH + CO$	1	1
1 4	$H_2 + HCNH^+ + C(OH)_2$	1	1
1 4	$2H + HNC + CH(OH)_2^+$	1	1
2	$NHCHCHOH^+ + H_2O$	5	3
2	$NH_2CHCHCOH + OH^+$	5	5
2	$NH_3CH_2CHO + O$	3	3
2	$NH_3CH_2CO + OH^+$	2	2
2	$NH_2CHCHO^+ + H_2O$	2	0
2	$NHCOHCH_2^+ + H_2O$	1	1
2 4	$2H_2 + C_2ON^+ + H_2O$	1	1
2 4	$H_2 + CNCHOH + H_2O$	1	1
2 4	$H_2 + NH_2CHCO + OH^+$	1	1
3	$NH_3 + CH_2COOH^+$	31	26
3	$NH_2^+ + CH_2C(OH)_2$	3	1
3	$NH + C(OH)_2CH_3^+$	2	2
3	$NH_4^+ + C_2O_2H_2$	1	1
3	$NH_4^+ + CHCOOH$	1	1
3 4	$H_2 + NOH^+ + COCH_2$	1	1
1 2	$NH_2CH_2^+ + CO + H_2O$	19	10
1 2	$NH_2CH_2 + CO + OH^+$	9	7
1 2	$HNC + CH_2OH^+ + H_2O$	6	6
1 2	$NHCH_2 + COH^+ + H_2O$	3	2
1 2	$NH_3CH^+ + CHO^+ + OH^-$	2	2
1 2	$NH_3CH_2 + COH^+ + O$	2	1
1 2	$NH_3CH^+ + CO + H_2O$	1	1
1 2	$CH_2OH^+ + CN^- + H_3O^+$	1	1
1 2	$CN + CH_2 + 2H_2O$	1	1
1 2	$HCN + HCHO + H_3O^+$	1	1
1 2	$HNC + HCHO + H_3O^+$	1	1
1 2	$NH_2C^+ + HCHO + H_2O$	1	1
1 2	$NH_2CH + COH^+ + H_2O$	1	1
1 2 4	$H_2 + HCNH^+ + CO + H_2O$	5	5
1 2 4	$H_2 + HCN + CO + H_3O^+$	4	4
1 2 4	$H^+ + NH_3CH_2 + CO + O$	3	3
1 2 4	$H_2 + HCN + CHO^+ + H_2O$	3	3
1 2 4	$H_2 + HNC + CO + H_3O^+$	2	2
1 2 4	$H + HNC + CHO\cdot + H_3O^+$	1	1
1 2 4	$H^+ + H_2 + HCNH^+ + CO + OH^-$	1	1
1 2 4	$H^+ + H_2 + HNC + CHO^+ + OH^-$	1	1
1 2 4	$H_2 + C_2N^+ + 2H_2O$	1	1
1 2 4	$H_2 + CN^+ + CHOH + H_2O$	1	1
1 2 4	$H_2 + CNH_2^+ + CO + H_2O$	1	1
1 2 4	$H_2 + HCN + COH^+ + H_2O$	1	1
1 2 4	$H_3^+ + CN\cdot + CHO\cdot + H_2O$	1	1
1 3	$NH_3 + CO + CH_2OH^+$	25	22
1 3	$NH_3 + HCOH + CHO^+$	4	3
1 3	$NH_2^+ + CO_2 + CH_4$	3	3
1 3	$NH + CO_2H^+ + CH_4$	2	2
1 3	$NH_3 + CO_2H^+ + CH_2$	2	2
1 3	$NH_3 + COH^+ + CHOH$	2	2
1 3	$NH + CH_2COH^+ + H_2O$	1	1
1 3	$NH_3 + CO_2 + CH_3^+$	1	1
1 3	$NH_4^+ + CO + CHOH$	1	1
1 3 4	$H_2 + NH_3 + CO + CHO^+$	6	6
1 3 4	$H_2 + NH_4^+ + 2CO$	3	3
1 3 4	$H_2 + CO_2H^+ + CH_3 + N$	2	2
1 3 4	$H + NH_2 + CO_2H + CH_2$	1	1
1 2 3	$NH_3 + COH^+ + H_2O + C$	2	2
1 2 3	$CHO^+ + CH_4 + OH\cdot + N$	1	1
1 2 3	$NH_3 + CO + H_3O^+ + C$	1	1
1 2 3 4	$H^+ + NH_3 + CHO\cdot + C + OH\cdot$	1	1
4	$H_2 + NH_2CHCOOH^+$	22	22
4	$2H_2 + C(OH)_2CN^+$	4	4
4	$H^+ + {}^+NH_3CH_2CO_2^-$	2	2
4	$H_2 + NHCHC(OH)_2^+$	2	2

[a]The grey cell indicates the charge distribution is uncertain.

Table 5
Products from gly-H^+ SID for $\theta_i = 45°$

Backbone cleavage pattern	Reaction channel[a]	Number of trajectories	Number of shattering
	No Reaction	81	
1	$NH_2CH_2^+ + C(OH)_2$	7	4
1	$NH_2CH_2^+ + HCOOH$	4	4
1	$NH_2C^+ + CH_2(OH)_2$	1	1
1	$NH_3CH^+ + HCOOH$	1	1
1	$CH_3NH_3^+ + CO_2$	1	1
1 4	$H_2 + NHCH_2 + CO_2H^+$	1	1
1 4	$H^- + NH_2CH_2^+ + CO_2H^+$	1	1
2	$NH_2CH_2CO^+ + H_2O$	1	0
3	$NH_3 + CH_2COOH^+$	12	8
3	$NH + C(OH)_2CH_3^+$	2	2
1 2	$NH_2CH_2^+ + CO + H_2O$	1	1
1 2 4	$H + NH_2CH_2 + CO + OH$	1	1
1 3	$NH_4^+ + CO_2 + CH_2$	1	0
4	$2H_2 + C(OH)_2CN^+$	1	1

[a]The grey cell indicates the charge distribution is uncertain.

channels is observed as shattering and non-shattering for the MP2 simulations at θ_i of 0° and 45°, except the one forming $NH_2CHCOOH^+ + H_2$, which is only observed at $\theta_i = 0°$ as shattering. It is also of interest that each of the 5 fragmentation channels were observed in the previous gly-H^+ AM1 simulations at $\theta_i = 45°$. For this previous AM1 study a total of 18 fragmentation channels (both shattering and non-shattering) were observed, while as shown in Table 5 a total of 14 fragmentation channels occurred for the current MP2 study. The larger number of fragmentation channels for the AM1 study may result from the longer period of time the unimolecular dynamics of the collisionally excited gly-H^+ ions are followed for this study as compared to the MP2 study; i.e., 1.3 ps versus 0.2–0.3 ps as shown in Table 5. Finally, the dominant fragmentation channel for both the MP2 and AM1 simulations is the formation of $NH_3 + CH_2COOH^+$. In future work it will be of interest to investigate the energetics of this channel by electronic structure calculations.

Table 6
Relative importance of different shattering channels

Shattering products	Percentage of all trajectories	
	MP2	AM1
$\theta_i = 0°$		
$NH_3 + CH_2COOH^+$	4.9[a]	–
$NH_3 + CO + CH_2OH^+$	4.2	–
$H_2 + NH_2CHCOOH^+$	4.2	–
$NH_2CH_2^+ + C(OH)_2$	2.3	–
$NH_2CH_2^+ + CO + H_2O$	1.9	–
$H_2 + NH_2CHOH^+ + CO$	1.7	–
$\theta_i = 45°$		
$NH_3 + CH_2COOH^+$	6.9[b]	1[c]
$NH_2CH_2^+ + C(OH)_2$	3.4	3
$NH_2CH_2^+ + HCOOH$	3.4	4
$NH + C(OH)_2CH_3^+$	1.7	0
$NHCH_2 + H_2 + COOH^+$	0.9	5

The collision energy is 70 eV = 1614 kcal/mol.
[a] Results of 527 trajectories.
[b] Results of 116 trajectories.
[c] Results of 100 trajectories.

QM + MM direct dynamics simulations, with AM1 as the model for V_{ion}, have been used to study gly_2-H^+ SID at the same collision energy and angle as considered in the current study; i.e., 70 eV and 0° [27]. Fewer fragmentation reaction channels, i.e., 44, were found for gly_2-H^+ as compared to the 96 found here for gly-H^+. This is an interesting result, since as shown in Table 3 the percentage fragmentation is nearly the same for gly-H^+ and gly_2-H^+. The same fraction of fragmentation for gly_2-H^+, via fewer channels, may result from the longer period of the time the unimolecular dynamics is followed for gly_2-H^+ as compared to gly-H^+. In future work it will be important to simulate gly_2-H^+ SID with MP2/6-31G* as is done here for gly-H^+.

5. Summary

In the work presented here a QM + MM direct dynamics simulation, with the MP2/6-31G* theory as a model for V_{ion} in Eq. (1), is used to study gly-H^+ + diamond {1 1 1} SID. The simulations are performed for collisions with incident angles $\theta_i = 0°$ (normal to the surface) and $\theta_i = 45°$, and a collision energy of 70 eV. The energy transfer and gly-H^+ fragmentation dynamics observed in this study are in accord with previous studies using both AMBER and AM1 for the ion's intramolecular potential V_{ion} [24].

A particularly important finding from the current study is that a significant fraction of the gly-H^+ ions fragment by a shattering mechanism as they collide with the surface. This result supports early studies [24,27] in which shattering fragmentation was also observed for both gly-H^+ and gly_2-H^+, in QM + MM direct dynamics simulations in which the AM1 semiempirical QM model was used for V_{ion}. The similarity between the AM1 and MP2 results suggests that it will be meaningful to use the more computationally efficient AM1 theory to model SID of much larger peptide ions, such as bradykinin for which shattering fragmentation is suggested from experimental studies [37–39]. It will be also important to consider other surfaces, such as a per-fluorinated self-assembled monolayer (F-SAM) and a model for this surface has been developed [56].

An issue which should be addressed in future work is the numerical instability of some of the direct dynamics trajectories. The instabilities arose from the MP2/6-31G* potential energy model for the gly-H^+ ion, and occurred in either the SCF convergence of the gly-H^+ potential energy or in a discontinuity in the gly-H^+ potential energy during the integration of the $\theta_i = 0°$ trajectories. This numerical instability was much less important for the $\theta_i = 45°$ trajectories and this difference apparently arises from the smaller amount of energy transferred to gly-H^+ for the oblique incident angle. For $\theta_i = 0°$, a total of 544 trajectories were calculated and 17 of them became unstable as gly-H^+ hit the surface. Thus, their possible fragmentation mechanisms and percent energy transfers could not be identified. For an additional 36 trajectories, gly-H^+ rebounded off the surface and fragmentation mechanisms could be identified. However, gly-H^+ or its fragmentation products were still strongly interacting with the surface. Thus, for these trajectories

it was not possible to determine the percent transfers of the initial collision energy to the surface and the gly-H^+ internal degrees. The fraction of these trajectories, i.e., $17/544 = 0.03$ and $(17 + 36)/544 = 0.10$, are not large and will not have a significant effect on the results. However, it is possible that there could be an interesting fragmentation event amongst the 17 trajectories whose fragmentations could not be analyzed, and the amount of energy transfer to gly-H^+ vibration may be particularly high for the 53 trajectories whose percent energy transfers could not be determined. Clearly it is important to accurately calculate the trajectory for each initial condition chosen by the sampling protocol. In future work it will be important to identify the origin(s) of the numerical instability in the MP2/6-31G* calculation for this direct dynamics simulation. Finally, we note that the trajectories calculated with the 6th order symplectic integrator [48] became more stable when the integration time step was reduced from 2 to 1 fs. It will be of interest to consider even smaller time steps and also different integrators in future work.

Acknowledgements

This material is based upon work supported by the National Science Foundation under Grants No. 0412677 and 0615321, and the Robert A. Welch Foundation under Grant No. D-0005.

References

[1] M.A. Mabud, M.J. Dekrey, R.G. Cooks, Int. J. Mass Spectrom. Ion Process. 67 (1985) 285.
[2] A.L. McCormack, Á. Somogyi, A.R. Dongré, V.H. Wysocki, Anal. Chem. 65 (1993) 2859.
[3] J.A. Burroughs, S.B. Wainhaus, L. Hanley, J. Phys. Chem. 98 (1994) 10913.
[4] J. Kubišta, Z. Dolejšek, Z. Herman, Eur. Mass Spectrom. 4 (1998) 311.
[5] J. Laskin, E. Densiov, J. Futrell, J. Am. Chem. Soc. 122 (2000) 9703.
[6] J.L. Jones, A.R. Dongré, Á. Somogyi, V.H. Wysocki, J. Am. Chem. Soc. 116 (1994) 8368.
[7] R.G. Cooks, T. Ast, M.A. Mabud, Int. J. Mass Spectrom. Ion Process. 100 (1990) 209.
[8] W. Aberth, Anal. Chem. 62 (1990) 609.
[9] M.E. Bier, J.C. Schwartz, K.L. Schey, R.G. Cooks, Int. J. Mass Spectrom. Ion Process. 103 (1990) 1.
[10] E.R. Williams, K.D. Henry, F.W. McLafferty, J. Shabanowitz, D.F. Hunt, J. Am. Soc. Mass Spectrom. 1 (1990) 413.
[11] R.B. Cole, S. Lemeillour, J.C. Tabet, Anal. Chem. 64 (1992) 365.
[12] A.L. McCormack, J.L. Jones, V.H. Wysocki, J. Am. Soc. Mass Spectrom. 3 (1992) 859.
[13] A.D. Wright, D. Despeyroux, K.R. Jennings, S. Evans, A. Riddoch, Org. Mass Spectrom. 27 (1992) 525.
[14] M. Meot-Ner (Mautner), A.R. Dongré, Á. Somogyi, V.H. Wysocki, Rapid Commun. Mass Spectrom. 9 (1995) 829.
[15] V.H. Wysocki, J.L. Jones, Á. Somogyi, A.L. McCormack, Biological Mass Spectrometry: Present and Future, Wiley, New York, 1994, p. 249.
[16] R.A. Chorush, D.P. Little, S.C. Beu, T.D. Wood, F.W. McLafferty, Anal. Chem. 67 (1995) 1042.
[17] K.L. Schey, D.A. Durkin, K.R. Thornburg, J. Am. Soc. Mass Spectrom. 6 (1995) 257.
[18] A.R. Dongré, Á. Somogyi, V.H. Wysocki, J. Mass Spectrom. 31 (1996) 339.
[19] A.R. Dongre, Á. Somogyi, V.H. Wysocki, J. Am. Chem. Soc. 118 (1996) 8365.
[20] D.G. Schultz, S.B. Wainhaus, L. Hanley, P. de Sainte Claire, W.L. Hase, J. Chem. Phys. 106 (1997) 10337.
[21] S.B.M. Bosio, W.L. Hase, Int. J. Mass Spectrom. Ion Process. 174 (1998) 1.
[22] O. Meroueh, W.L. Hase, Phys. Chem. Chem. Phys. 3 (2001) 2306.
[23] O. Meroueh, W.L. Hase, J. Am. Chem. Soc. 124 (2002) 1524.
[24] S.O. Meroueh, Y. Wang, W.L. Hase, J. Phys. Chem. A 106 (2002) 9983.
[25] K. Song, O. Meroueh, W.L. Hase, J. Chem. Phys. 118 (2003) 2893.
[26] J. Wang, S.O. Meroueh, Y. Wang, W.L. Hase, Int. J. Mass Spectrom. 230 (2003) 57.
[27] Y. Wang, W.L. Hase, K. Song, J. Am. Soc. Mass Spectrom. 14 (2003) 1402.
[28] A. Rahaman, J.B. Zhou, W.L. Hase, Int. J. Mass Spectrom 249–250 (2006) 321.
[29] A. Rahaman, O. Collins, C. Scott, J. Wang, W.L. Hase, J. Phys. Chem. A 110 (2006) 8418.
[30] J. Laskin, E. Denisov, J.H. Futrell, J. Phys. Chem. B 105 (2001) 1895.
[31] J. Laskin, J.H. Futrell, J. Chem. Phys. 116 (2002) 4302.
[32] J. Laskin, J.H. Futrell, J. Chem. Phys. 119 (2003) 3413.
[33] A. Rahaman, K. Song, J. Wang, S.O. Meroueh, W.L. Hase, in: C. Lifshitz, J. Laskin (Eds.), Principles of Mass Spectrometry Applied to Biomolecules, Wiley, New York, 2006, p. 379.
[34] T. Baer, W.L. Hase, Unimolecular Reaction Dynamics. Theory and Experiments, Oxford, New York, 1996, p. 171.
[35] J.A. Burroughs, S.B. Wainhaus, L. Hanley, J. Phys. Chem. 103 (1995) 6706.
[36] D.G. Schultz, L. Hanley, J. Chem. Phys. 109 (1998) 10976.
[37] J. Laskin, T.H. Bailey, J.H. Futrell, J. Am. Chem. Soc. 125 (2003) 1625.
[38] J. Laskin, J.H. Futrell, J. Am. Soc. Mass Spectrom. 14 (2003) 1340.
[39] J. Laskin, J.H. Futrell, Mass Spectrom. Rev. 22 (2003) 158.
[40] K. Bolton, W.L. Hase, G.H. Peslherbe, in: D.L. Thompson (Ed.), Multidimensional Molecular Dynamics Methods, World Scientific, London, 1998, p. 143.
[41] L. Sun, W.L. Hase, in: K.B. Lipkowitz, R. Larter, T.R. Cundari (Eds.), Reviews in Computational Chemistry, vol. 19, Wiley, New York, 2003, p. 79.
[42] K.C. Hass, M.A. Tamor, T.R. Anthony, W.F. Banholzer, Phys. Rev. B 45 (1992) 7171.
[43] B. Deb, K. Song, W.L. Hase, in preparation.
[44] W.L. Hase, R.J. Duchovic, X. Hu, A. Komornicki, K.F. Lim, D.-H. Lu, G.H. Peslherbe, K.N. Swamy, S.R. Vande Linde, L. Zhu, A. Varandas, H. Wang, R.J. Wolf, Quant. Chem. Prog. Exch. (QCPE) Bull. 16 (1996) 671.
[45] M.J. Frisch, G.W. Trucks, H.B. Schlegel, G.E. Scuseria, M.A. Robb, J.R. Cheeseman, J.A. Montgomery Jr., T. Vreven, K.N. Kudin, J.C. Burant, J.M. Millam, S.S. Iyengar, J. Tomasi, V. Barone, B. Mennucci, M. Cossi, G. Scalmani, N. Rega, G.A. Petersson, H. Nakatsuji, M. Hada, M. Ehara, K. Toyota, R. Fukuda, J. Hasegawa, M. Ishida, T. Nakajima, Y. Honda, O. Kitao, H. Nakai, M. Klene, X. Li, J.E. Knox, H.P. Hratchian, J.B. Cross, V. Bakken, C. Adamo, J. Jaramillo, R. Gomperts, R.E. Stratmann, O. Yazyev, A.J. Austin, R. Cammi, C. Pomelli, J.W. Ochterski, P.Y. Ayala, K. Morokuma, G.A. Voth, P. Salvador, J.J. Dannenberg, V.G. Zakrzewski, S. Dapprich, A.D. Daniels, M.C. Strain, O. Farkas, D.K. Malick, A.D. Rabuck, K. Raghavachari, J.B. Foresman, J.V. Ortiz, Q. Cui, A.G. Baboul, S. Clifford, J. Cioslowski, B.B. Stefanov, G. Liu, A. Liashenko, P. Piskorz, I. Komaromi, R.L. Martin, D.J. Fox, T. Keith, M.A. Al-Laham, C.Y. Peng, A. Nanayakkara, M. Challacombe, P.M.W. Gill, B. Johnson, W. Chen, M.W. Wong, C. Gonzalez, J.A. Pople, Gaussian 03, Revision C.02, Gaussian Inc., Wallingford CT, 2004.
[46] G.H. Peslherbe, H. Wang, W.L. Hase, in: D.M. Ferguson, J.I. Siepman, D.G. Truhlar (Eds.), Monte Carlo Methods in Chemical Physics, Advances in Chemical Physics, vol. 105, Wiley, New York, 1999, p. 171.
[47] M.P. Allen, D.J. Tildesley, Computer Simulation of Liquids, Oxford, New York, 1987.
[48] Ch. Schlier, A. Seiter, Comp. Phys. Commun. 130 (2000) 176.
[49] B. Balta, M. Basma, V. Aviyente, C. Zhu, C. Lifshitz, Int. J. Mass Spectrom. 201 (2000) 69.

[50] R.A.J. O'Hair, P.S. Broughton, M.L. Styles, B.T. Frink, C.M. Hadad, J. Am. Soc. Mass Spectrom. 11 (2000) 687.
[51] F. Rogalewicz, Y. Hoppilliard, Int. J. Mass Spectrom. 199 (2000) 235.
[52] F. Rogalewicz, Y. Hoppiliiard, G. Ohanessian, Int. J. Mass Spectrom. 195/196 (2000) 565.
[53] A.G. Harrison, T. Yalcin, Int. J. Mass Spectrom. Ion Process. 165/166 (1997) 339.
[54] S. Beranova, J. Cai, C. Wesdemiotis, J. Am. Chem. Soc. 117 (1995) 9492.
[55] J.S. Klassen, P. Kebarle, J. Am. Chem. Soc. 119 (1997) 6552.
[56] E. Martínez-Nuñez, A. Rahaman, W.L. Hase, J. Phys. Chem. C 111 (2007) 354.